RSC Advances

PAPER

View Article Online
View Journal | View Issue

Cite this: *RSC Adv.*, 2016, **6**, 52665

Soft template inducted hydrothermal $BiYO_3$ catalysts for enhanced formic acid formation from the photocatalytic reduction of carbon dioxide

Zuzeng Qin,*[ab] Hui Tian,[a] Tongming Su,[a] Hongbing Ji[ac] and Zhanhu Guo*[b]

Received 4th February 2016
Accepted 19th May 2016

DOI: 10.1039/c6ra03340g

www.rsc.org/advances

Bismuth yttrium oxide ($BiYO_3$) photocatalysts were hydrothermally prepared using sodium dodecyl benzene sulfonate (SDBS), disodium ethylenediamine tetraacetate (EDTA), and citric acid (CA) as soft templates. The effects of templates on the formed $BiYO_3$ nanostructures were revealed. The $BiYO_3$ nanostructures prepared without the existing template and with the existence of SDBS, EDTA, and CA as templates had flaked structures, sliced, rectangular lath structures with fine particles, and scaly uniform particles, respectively. The photocatalytic reduction of CO_2 under visible-light irradiation with these synthesized $BiYO_3$ nanostructures was studied and compared. Due to the larger specific surface area, higher adsorbed edge, and lower band gap, $BiYO_3$ prepared using EDTA as a template produced fewer hydroxyl free radicals (·OH) to give a higher yield of formic acid (HCOOH) in the process of the photocatalytic reduction of CO_2. The HCOOH yield from the photocatalytic reduction of CO_2 by the EDTA synthesized $BiYO_3$ was 1.68 μmol L^{-1}, which was 1.9 times higher than that produced from $BiYO_3$ prepared without a template, and 2.6 times higher than that of $BiYO_3$ prepared by a solid-state reaction.

1. Introduction

With accelerated industrialization and urbanization processes and continuously upgraded consumption structures, CO_2 generated from the combustion of coal, oil, natural gas and other hydrocarbon fuels has increased unbelievably over the past decade, and the subsequent energy crisis and global warming have become increasingly serious.[1,2] Therefore, it is very urgent to transform and utilize CO_2. At present, the conversion technology of CO_2 includes biological,[3] electrochemical,[4] photochemical,[5] and photocatalytic reduction[6] methods. Due to the required clean and renewable solar energy, mild reaction conditions, and lack of pollution, the photocatalytic reduction is considered favorably for CO_2 conversion to valuable chemicals.

The photocatalytic conversion of CO_2 into hydrocarbons uses solar energy to excite semiconductor photocatalysts to produce photogenerated electron–hole pairs and to induce a redox reaction to synthesize hydrocarbons from CO_2.[7–8] For example, Halmann[9] used GaP as a photoelectric pole to reduce CO_2 to CH_3OH in an aqueous solution in 1978. Inoue *et al.* used TiO_2, CdS, GaP, ZnO, and SiC photocatalysts to photocatalytically reduce CO_2 in 1979.[10] TiO_2 is the most popular material used in the photocatalytic reduction of CO_2, however, the band gap of TiO_2 is 3.2 eV, which can only respond to ultraviolet light (UV) (about 3–5% in the solar light) for the photocatalytic reaction. In recent years, to utilize visible light, modification of TiO_2 with Ag,[11] Cu_2O,[12] and CeO_2 [13] has been reported to shift the absorption edge of TiO_2 from the UV range to the visible light range. On the other hand, developed new "second generation" photocatalysts have been used in the photocatalytic reduction of CO_2, such as Zn_2GeO_4,[14] HNb_3O_8,[15] $ZnGa_2O_4$,[16] and $BiVO_4$.[17] Although the photocatalytic reduction of CO_2 has made significant progress, there are still many problems, for example, the low utilization rate of solar energy, low quantum yield, low adsorption of CO_2 on the photocatalyst, and poor light stability. All these lead to a very low yield of hydrocarbons. Meanwhile, a template can effectively control crystal nucleation, growth and the assembly process of inorganic materials by simulating the biological mineralization process, and subsequently can influence the surface morphology, catalyst particle size and the interaction between the photocatalyst and the reactant.[20,25] Bi-based oxide semiconductors have unique electronic structures, forming a valence band between the Bi-6s and the O-2p,[18] for example, $BiVO_4$,[19] Bi_2MoO_6,[20] $BiWO_6$,[21] and $BiYO_3$.[22–23] However, their application for the photocatalytic reduction of CO_2 has rarely been reported.

In this work, $BiYO_3$ photocatalysts were prepared using a hydrothermal method. The influence of a soft template

[a]*School of Chemistry and Chemical Engineering, Guangxi Key Laboratory of Petrochemical Resource Processing and Process Intensification Technology, Guangxi University, Nanning 530004, China. E-mail: qinzuzeng@gmail.com*

[b]*Integrated Composites Laboratory (ICL), Department of Chemical and Biomolecular Engineering, University of Tennessee, Knoxville, Tennessee 37966, USA. E-mail: zguo10@utk.edu*

[c]*Department of Chemical Engineering, School of Chemistry & Chemical Engineering, Sun Yat-sen University, Guangzhou 510275, China*

sodium dodecyl benzene sulfonate (SDBS), disodium ethylenediamine tetraacetate (EDTA), and citric acid (CA) on the photocatalysts were studied. The photocatalytic reduction of CO_2 conversion was studied and compared.

2. Experimental

2.1. Preparation of photocatalysts

The $BiYO_3$ photocatalysts with different templates were prepared by a hydrothermal method. Briefly, 0.5 mol L^{-1} $Bi(NO_3)_3$ aqueous solution and 0.5 mol L^{-1} $Y(NO_3)_3$ aqueous solution were mixed evenly. Then, 4 mol L^{-1} NH_4OH was added into the mixture with stirring at 100 rpm to adjust the pH = 8.0; after that 2.0 g SDBS, EDTA, or CA were added into the mixture as a template. After being stirred at room temperature for 0.5 h, the mixture was transferred into a Teflon-lined stainless sealed autoclave and heated at 180 °C for 12 h. After natural cooling, the reactant was vacuum filtrated and washed with deionized water, and then dried at 90 °C for 10 h and calcined at 700 °C for 2 h to obtain $BiYO_3$. The $BiYO_3$ prepared by SDBS, EDTA, and CA were marked as $BiYO_3$-SDBS, $BiYO_3$-EDTA, and $BiYO_3$-CA, respectively. For comparison, the $BiYO_3$ catalyst (marked as $BiYO_3$-blank) was prepared following the same method without adding a template. Meanwhile, the $BiYO_3$ catalyst was further prepared by a solid state reaction following the prior procedures for comparison.[22]

2.2. Photocatalytic activity tests

The photocatalytic reduction of CO_2 was carried out in a SGY-I photochemical reactor (Nanjing Stonetech Electric Equipment Co., Ltd.). A 300 W Xe lamp was used as the light source and the UV light was removed by UV cut-off filter. 200 mL NaOH (0.25 mol L^{-1}) and Na_2SO_3 (0.1 mol L^{-1}) aqueous solution was used to maintain an alkaline environment in the reaction process, and 2.00 g L^{-1} $BiYO_3$ catalysts were added into the reactor. Before illuminating, CO_2 was allowed to flow into the reactor at 100 mL min^{-1} for 0.5 h with solution stirring to reach an absorption equilibrium. During the reaction process, about 5 mL of the reaction suspension was extracted every 1.0 h. The products, mainly formic acid (HCOOH), were detected by a TU-1901 dual beam UV-visible spectrophotometer (Beijing Purkinje General Instrument Co., Ltd) according to the method described in the literature.[24]

2.3. Characterizations and measurements

XRD was conducted on a Bruker D8 Advance X-ray diffractometer with Cu Kα radiation at 36 kV, 55 mA using a graphite monochromator. The morphology of the photocatalysts was investigated using a Hitachi SU-8020 scanning electron microscope (SEM). The oxidation state and surface composition were analyzed using an X-ray photoelectron spectrometer (XPS) (Kratos Ultra Axis DLD), equipped with an Al Kα radiation source, and the XPS analysis was conducted at 150 W with a pass energy of 40 eV. The Fourier transform infrared (FTIR) spectrum of $BiYO_3$ samples was studied in a Nicolet NEXUS 470 infrared spectrometer (Thermo Nicolet, USA), and $BiYO_3$ was pressed into a tablet after being dispersed in a KBr matrix, and scanned 20 times at a resolution of 4 cm^{-1} from 400 to 4000 cm^{-1}. The N_2 adsorption/desorption was conducted using a Micromeritics TriStar II 3020 surface area and porosity analyzer with N_2 (at 77.3 K) as sorbate, the total specific surface areas were calculated by the multi-point Brunauer–Emmett–Teller (BET) method and the pore size distributions were evaluated using the standard Barrett–Joyner–Halenda (BJH) method. The UV-vis diffuse reflection spectra of the catalysts were collected by a TU-1901 dual beam UV visible spectrophotometer (Beijing Purkinje General Instrument Co., Ltd.), and were converted from reflectance to absorbance by the Kubelka–Munk method. A photoluminescence (PL) technique with terephthalic acid as a probe molecule was used to detect the formation of ·OH free radicals on the surface of the UV-illuminated photocatalyst, the details of the PL test were documented elsewhere.[25] The zeta potentials of the $BiYO_3$ samples were obtained in a Zeta Potential Analyzer (BrookHaven, American) in 0.1 mM KCl aqueous solution and at 25 °C.

3. Results and discussion

3.1. XRD and zeta potential analysis

Fig. 1 shows the XRD patterns of the $BiYO_3$ photocatalysts prepared by SDBS, EDTA and CA and with no template using a hydrothermal method after being calcined at 700 °C for 2 h. The XRD patterns of the four photocatalysts can be indexed to $BiYO_3$ (JCPDF card no. 27-1047); the peaks at 2θ = 28.58°, 33.01°, 47.36°,56.14°, 58.85°, 69.06°, 76.44°, and 78.69° corresponded to the crystal planes of (111), (200), (220), (311), (222), (400), (331), and (420) of $BiYO_3$, respectively, indicating that $BiYO_3$ can be obtained by a hydrothermal method with SDBS, EDTA, and CA as a template or without a template.

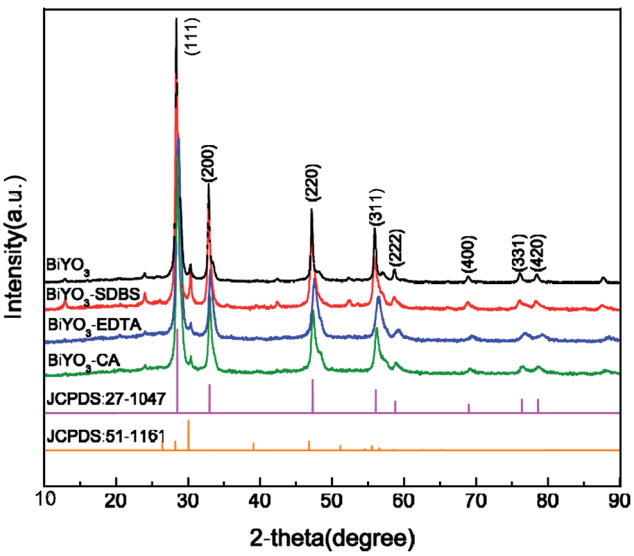

Fig. 1 XRD patterns of the $BiYO_3$ photocatalysts prepared by SDBS, EDTA and CA and without template using a hydrothermal method.

A weak diffraction peak observed in all the four samples was found at $2\theta = 30.40°$, attributed to the diffraction peak of Bi_2O_3, which was the intermediate product during the hydrothermal reaction process. The formation of Bi_2O_3 would consume the Bi^{3+} ions, leading to a decreased Bi^{3+} concentration in the reaction solution. A lower concentration of the reactants (Bi^{3+}) can promote the growth of the $BiYO_3$ crystal.[26] The diffraction peak of the $BiYO_3$ photocatalyst without a template was narrow, while the diffraction peaks of the $BiYO_3$ photocatalysts prepared with adding SDBS, EDTA, and CA were slightly wide. A decreasing grain size of crystallite was observed using Scherrer's equation according to the $BiYO_3$ (111) peaks, the crystallite sizes of photocatalysts were 21.44, 18.42, 18.02, and 16.34 nm, respectively.

The interactions between the adsorbents and the $BiYO_3$ samples strongly depend on the surface charge of the templates. The zeta potentials of the surface charged particles were measured and are shown in Table 1. The zeta potential of the $BiYO_3$ prepared using SDBS, EDTA, and CA as templates was 2.98, 4.70 and 3.09 mV, respectively, lower than that of the $BiYO_3$ prepared by no template (16.47 mV). This indicates that the addition of anionic surfactant caused a decrease of the zeta potential.[27] SDBS and CA are anionic surfactants, and EDTA is a chelate with four carboxyl groups, which may easily dissociate negative charge. The decreased zeta potential for the $BiYO_3$ prepared using SDBS, EDTA, and CA as templates with adsorbed positive and negative charges had a significant effect on the crystallite size.[28] This indicates that the template has a structure directing effect on the formed $BiYO_3$ during its crystal nucleation and growth in the reaction process. According to the measured zeta potential value, the stronger the adsorption force between the template and $BiYO_3$, the more the inhibition of the crystal growth, and thus, the crystallite size of $BiYO_3$ after adding SDBS, EDTA, and CA was decreased.

3.2. SEM analysis

Fig. 2 shows SEM images of the $BiYO_3$ photocatalysts prepared with no template, and with SDBS, EDTA, and CA as templates by a hydrothermal method. As shown in Fig. 2(a), the $BiYO_3$ photocatalyst prepared without template was flaky with a flake length of 100–600 nm. In Fig. 2(b) it can be seen that the $BiYO_3$ prepared using SDBS as a template formed slices with a length of 100–800 nm and a thickness of about 10 nm. SDBS is an anionic surface active agent and can produce negatively charged surface active agents in aqueous solution. These adsorbed negative charges cover the photocatalyst surface to promote the crystal growth and form a thin slice.[26] In Fig. 2(c) it can be seen that the $BiYO_3$ catalysts prepared using EDTA as a template showed a rectangular lath structures with fine particles with size less than 10 nm on the surface, different from the $BiYO_3$ catalysts formed with SDBS. When the chelating agent EDTA with six atoms was added into the aqueous solution, the Bi–EDTA chelate compound decreased the concentration of free Bi^{3+} in the solution, slowed down the growth rate of $BiYO_3$ crystal,[29] and thus generated tiny nanoparticles[26] with uniform dispersion. When the photocatalytic reaction was carried out, the edge of the rectangular lath structure serves as sites for electronic transition, and thus an accelerated photocatalytic reaction was observed on the $BiYO_3$ powders. In Fig. 2(d) it can be seen that the $BiYO_3$ photocatalyst prepared using CA as a template formed scaly uniform particles. When the complexing agent CA with three carboxyl groups was added into the solution, three H^+ were dissociated and the complex compound of –COOBi would be formed to promote the growth rate of $BiYO_3$ crystal.[30]

Table 1 The effects of the type of template on the zeta potential

Sample name	Zeta potential (mV)
$BiYO_3$-blank	16.47
$BiYO_3$-SDBS	2.98
$BiYO_3$-EDTA	4.70
$BiYO_3$-CA	3.09

3.3. XPS analysis

The elementary oxidation states and surface composition of $BiYO_3$ prepared without template, and with SDBS, EDTA and CA as templates were investigated using XPS analysis, Fig. 3. The binding energies of the core electrons of the four $BiYO_3$ photocatalysts are shown in Table 2. In the Bi 4f spectrum, the binding energy of Bi 4f7/2 in the four samples was about 164 and 156 eV,[31] and the binding energy of Bi 4f5/2, a weak peak, was 156 eV,[32] suggesting that Bi occurred in the form of Bi^{3+} in $BiYO_3$. As shown in Table 2, with the addition the template of SDBS, EDTA, or CA, the binding energies of Bi 4f7/2 and Bi 4f5/2 of $BiYO_3$ had a blue shift of 0.1 eV. As mentioned previously, SDBS, an anionic surface active agent, can produce negative charges in aqueous solutions and absorb on the surface of the photocatalyst, increasing the extra nuclear electron density of the Bi atomic nucleus. The chelating agent EDTA with six atoms can form Bi–EDTA chelates with Bi^{3+} in alkaline conditions; the complexing agent CA with three carboxyl groups can dissociate and give three H^+ in water, and form three –COOBi complexes with Bi^{3+} ions. When the chemical bonds were formed between the Bi atom and EDTA or CA, the nuclear electron density of Bi increases and the binding energy decreases due to the transfer of valence electron to the Bi.[33] For the Y 3p spectra in Fig. 3, the Y 3p3/2 (312 eV) and Y 3p1/2 (300 eV) of the catalysts after using three templates were similar to the catalysts without template and could be assigned to the surface of Y^{3+} species.[34] In the O 1s spectrum, three kinds of binding oxygen were observed, namely, (a) oxygen in the lattice (O^{2-}) located at 529.3 eV,[35] (b) oxygen in the hydroxyl group on the photocatalysts surface (–OH) located at 531.4 eV,[36] and (c) oxygen absorbed on the surface (O^-) located at 533.2 eV.[35–36] From the spectra and the data in Table 2, the content of surface adsorbed oxygen of the $BiYO_3$ prepared by EDTA (0.92%) was significantly lower than that of the other three kinds of catalysts.

In a photocatalytic reaction, the oxygen species played an important role in the reaction process.[37–38] Especially, in a photocatalytic reduction reaction system, the adsorbed oxygen species can be used as the electron acceptor to compete for the

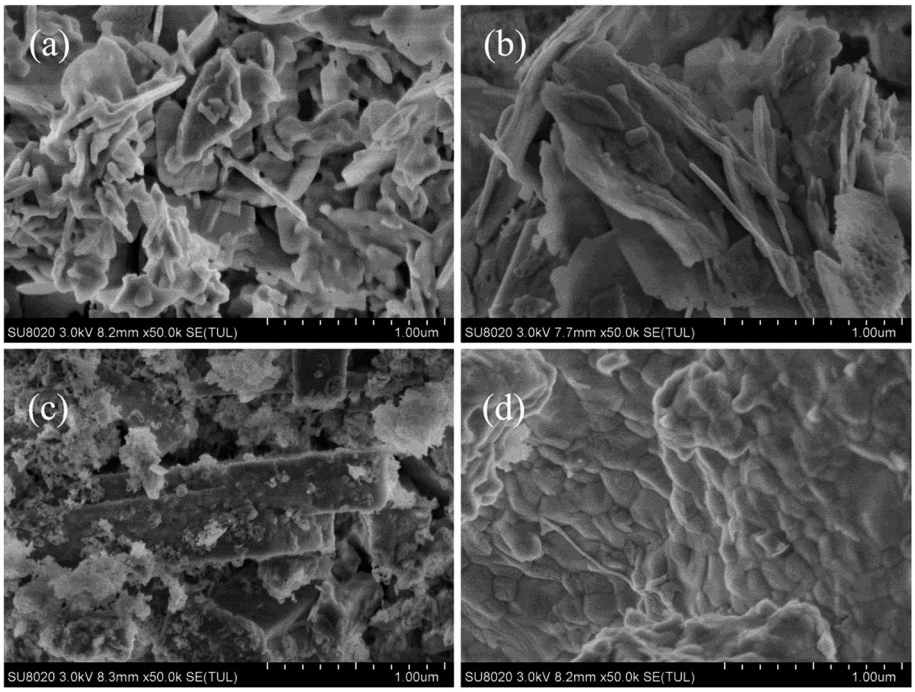

Fig. 2 SEM images of the $BiYO_3$ catalysts prepared (a) without any template, and with a template of (b) SDBS, (c) EDTA, and (d) CA using a hydrothermal method.

photoelectron, thus the presence of adsorbed oxygen species will prevent the photocatalytic reduction reaction.[39] The oxygen species of chemical adsorption, such as surface hydroxyl groups, are scavengers of photo-induced holes and can generate active species ·OH free radicals. The ·OH in the adsorbed phase and solution phase is a strong oxidant and can easily initiate an oxidation reaction. The physically adsorbed oxygen species, such as O_2, act as scavengers of the photo-induced electrons. Thus, an increased amount of the physically adsorbed oxygen would help to improve the capture of the photo-induced electrons and decrease the recombination probability of the photo-induced electrons and the photo-induced holes, which will inhibit the photocatalytic reduction reaction. The total adsorbed oxygen species (including the surface hydroxyl oxygen and surface adsorbed oxygen) content of $BiYO_3$ prepared with no template, and using SDBS, EDTA, and CA as templates were 38.9%, 51.6%, 48.84%, and 51.32%, respectively.

3.4. N_2 adsorption–desorption analysis

Fig. 4 shows N_2 adsorption–desorption isotherms and the pore size distribution curves of the different $BiYO_3$ catalysts. The

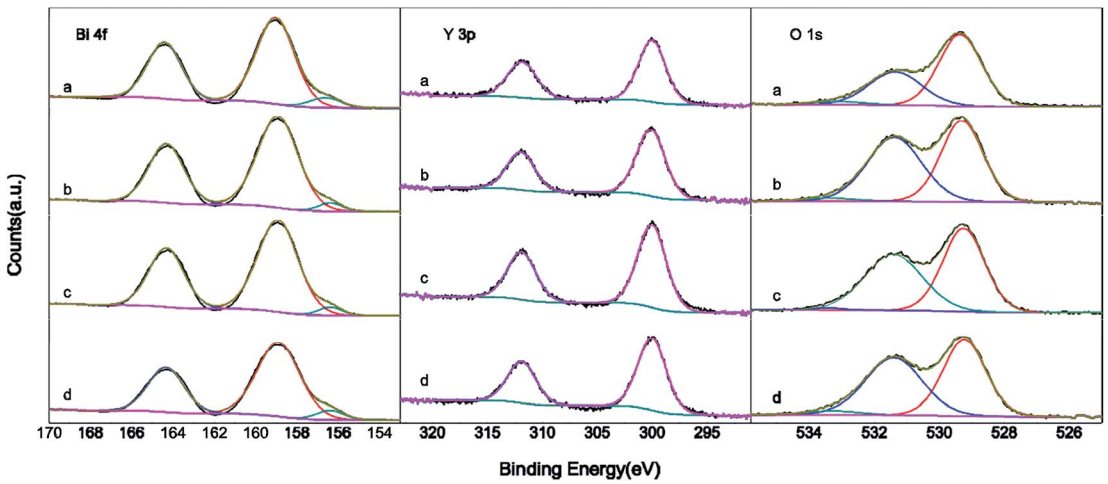

Fig. 3 The Bi 4f, Y 3p, and O 1s XPS spectra of $BiYO_3$ prepared (a) without template, and with a template of (b) SDBS, (c) EDTA, and (d) CA by a hydrothermal method.

Table 2 Binding energy (BE, eV) of core electrons of $BiYO_3$ catalysts prepared by using SDBS, EDTA, and CA as template and no template by a hydrothermal method

		BE (percent of valence state, %)			
XPS spectra	Element valence	$BiYO_3$-blank	SDBS-$BiYO_3$	EDTA-$BiYO_3$	CA-$BiYO_3$
Bi 4f	Bi^{3+}(Bi 4f7/2)	164.41(34.63)	164.32 (34.75)	164.34(31.50)	164.33(32.06)
	Bi^{3+}(Bi 4f5/2)	159.03(59.67)	158.92(62.07)	158.91(61.91)	158.90(62.94)
	Bi^{3+}(Bi 4f7/2)	156.61(5.71)	156.38(3.19)	156.54(6.59)	156.38(5.00)
Y 3p	Y^{3+}(Y 3p3/2)	311.89(38.28)	311.98(35.60)	311.91(36.57)	311.90(36.35)
	Y^{3+}(Y 3p1/2)	300.03(61.72)	300.12(64.40)	300.03(63.43)	300.02(63.65)
O 1s	OH^-	531.36(35.18)	531.39(49.53)	531.44(47.92)	531.41(48.51)
	O^-	533.16(3.72)	533.39(2.07)	533.20(0.92)	533.28(2.80)
	O^{2-}	529.36(61.10)	529.31(48.40)	529.26(51.16)	529.23(48.68)

specific surface areas of the different $BiYO_3$ photocatalysts obtained by a multi-point BET method and other parameters are shown in Table 3. It can be found that the N_2 adsorption isotherm of the four samples belonged to a III-type isotherm with an H3-type hysteresis loop. At low pressures ($P/P_0 = 0$–0.8), the adsorption capacity of N_2 increased slowly with increasing relative pressure, indicating that the adsorption of N_2 molecules on the surface of catalyst was converted to a multi-layer adsorption.[40] At high pressures ($P/P_0 = 0.8$–1.0), the isotherms obtained by desorption were not coincident with the adsorption isotherms, attributed to the occurrence of capillary condensation. From Fig. 4(A) it can be seen that the hysteresis loop of $BiYO_3$ prepared using EDTA as template began at $P/P_0 = 0.8$ and ended at P/P_0 of about 1.0, the beginning relative pressure was 0.05 lower that other samples, indicating that the amount of adsorption and desorption by the $BiYO_3$ prepared using EDTA as template was larger than that of other catalysts according to the capillary condensed theory and Kelvin equation.[41]

As shown in Fig. 4(B) and Table 2, the four $BiYO_3$ photocatalysts were mesoporous. The pore size of $BiYO_3$ prepared without a template was 4.72 nm, while it was 2.14, 20.20, and 30.17 nm for the $BiYO_3$ prepared using SDBS, EDTA, and CA as templates, respectively, showing that the templates had a significant effect on the pore size of the photocatalyst.[42]

The specific surface areas of $BiYO_3$ prepared using SDBS, EDTA, and CA are 15.62, 20.87, and 12.20 $m^2\ g^{-1}$, respectively, which are higher than that of the $BiYO_3$ prepared without a template (6.75 $m^2\ g^{-1}$). Obviously, after using templates, the surface areas and pore volume of $BiYO_3$ were increased. Among these samples, the $BiYO_3$ prepared using EDTA as template had a larger specific surface area and a bigger pore volume than the other three $BiYO_3$ samples.

3.5. UV-vis diffuse reflectance spectra and FTIR analysis

Fig. 5 shows the UV-vis diffuse reflectance spectra and the FTIR spectra of $BiYO_3$ prepared without a template, and using SDBS, EDTA, and CA as templates with a hydrothermal method. Obviously, these four $BiYO_3$ samples absorbed visible light, and the absorbed edges of the $BiYO_3$ prepared without a template, and using SDBS, EDTA, and CA as templates were 517, 533, 569, and 539 nm, indicating that the adsorbed edges had a red shift after the templates were added. For a semiconductor sample, it is possible to determine the optical absorption near the band edge using a Kubelka–Munk method,[43] as show in eqn (1).

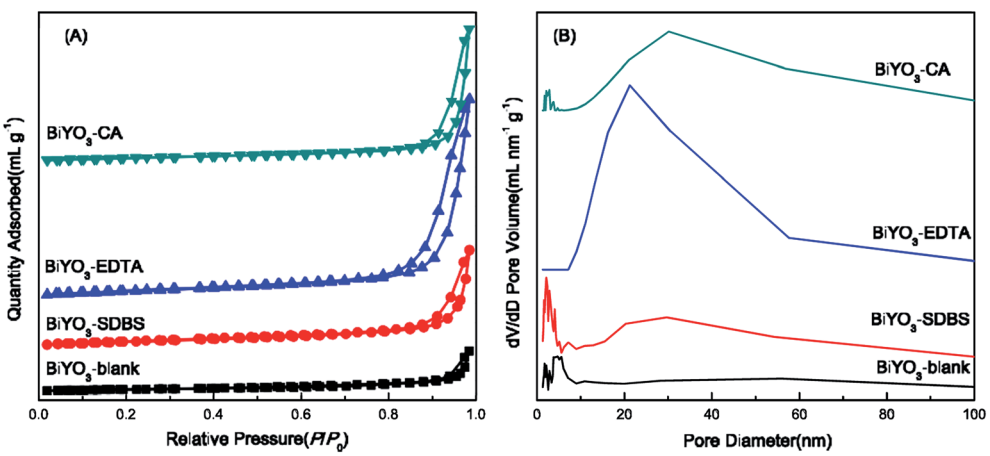

Fig. 4 (A) Nitrogen adsorption/desorption isotherms and (B) pore size distribution of $BiYO_3$ prepared by (a) no template and using (b) SDBS, (c) EDTA, and (d) CA as templates with a hydrothermal method.

Table 3 Textural properties of the $BiYO_3$ catalysts prepared using SDBS, EDTA, and CA as templates and no template with a hydrothermal method

Sample name	BET surface area ($m^2\ g^{-1}$)	Pore diameter (nm)	Pore volume ($mL\ g^{-1}$)
$BiYO_3$-blank	6.75	4.72	0.034
$BiYO_3$-SDBS	15.62	2.14	0.080
$BiYO_3$-EDTA	20.87	20.20	0.164
$BiYO_3$-CA	12.20	30.17	0.109

$$\alpha h\nu = A(h\nu - E_g)^{n/2} \quad (1)$$

where α is the absorption coefficient; ν is the radiation frequency; h is the Planck constant; A is a constant; and E_g is the band gap. According to eqn (1), the band gap values of the $BiYO_3$ prepared without a template, and using SDBS, EDTA, and CA as templates were 2.39, 2.32, 2.18, and 2.30 eV, respectively. After the introduction of a template, red shifts were observed on the three samples, because the Bi–EDTA or –COOBi covalent bonds were formed between Bi atom and three templates through the negative charges in the aqueous solution. Therefore, the transfer of valence electrons to the Bi atom and the hybrid orbital of Bi 6s and O 2p became narrow.[30] This increased the activity of photoelectrons and holes and electronic transition becomes easier after being photo-excited.

The FT-IR spectra (Fig. 5(B)) of the four samples show main absorption bands at 3440 and 1600 cm^{-1}, which correspond to the O–H stretching and H–O–H bending vibrations of the adsorbed moisture in the samples,[44] and the peaks at about 848 cm^{-1} were attributed to the stretching vibrations of the Bi–O in $BiYO_3$.[45] The weak bands at about 2990 and 2831 cm^{-1} were ascribed to the stretching vibrations of the aliphatic CH_2 and CH_3 groups,[27] respectively, which were not found in the spectrum of the $BiYO_3$ prepared without a template, indicating very small amount of the templates were found on the $BiYO_3$ surface. This further confirmed the zeta potential results.

3.6. Fluorescence spectroscopy analysis

The charges (electron e^- and hole h^+), photogenerated from the inside of the photocatalyst to the surface in a photocatalytic process, react with water to produce a very strong oxidation ability species, *i.e.*, hydroxyl radicals. Hydroxyl radicals are an important active species in preventing the activity of the photocatalytic reduction. The higher the content of hydroxyl radicals, the easier it is to capture the light, and the more difficult it is to undergo the photocatalytic reduction reaction.[46–47] Terephthalic acid reacts with hydroxyl groups readily to produce a highly fluorescent product, 2-hydroxyterephthalic acid, whose PL peak intensity is in proportion to the amount of hydroxyl radicals produced in water.[48] A photoluminescence (PL) technique with terephthalic acid as a probe molecule was used to detect the formation of free hydroxyl radicals on the surface of the $BiYO_3$ photocatalyst with different template agents, Fig. 6.

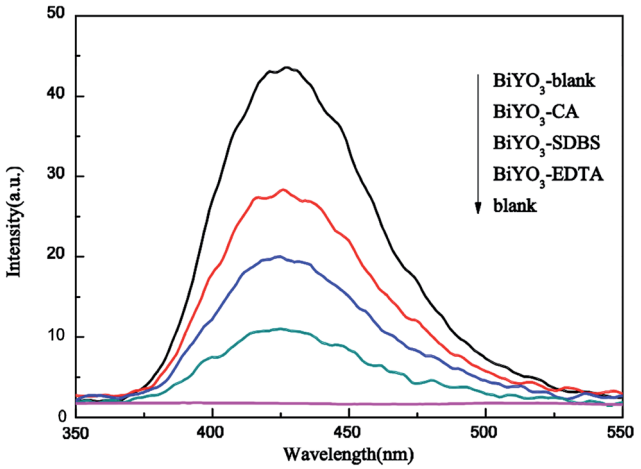

Fig. 6 PL spectra observed after illumination of $BiYO_3$ prepared by no template and using SDBS, EDTA, and CA as templates with a hydrothermal method in 2×10^{-3} mol L^{-1} NaOH solution of terephthalic acid (excitation at 315 nm), and the blank was the the fluorescence spectrum of pureterephthalic acid.

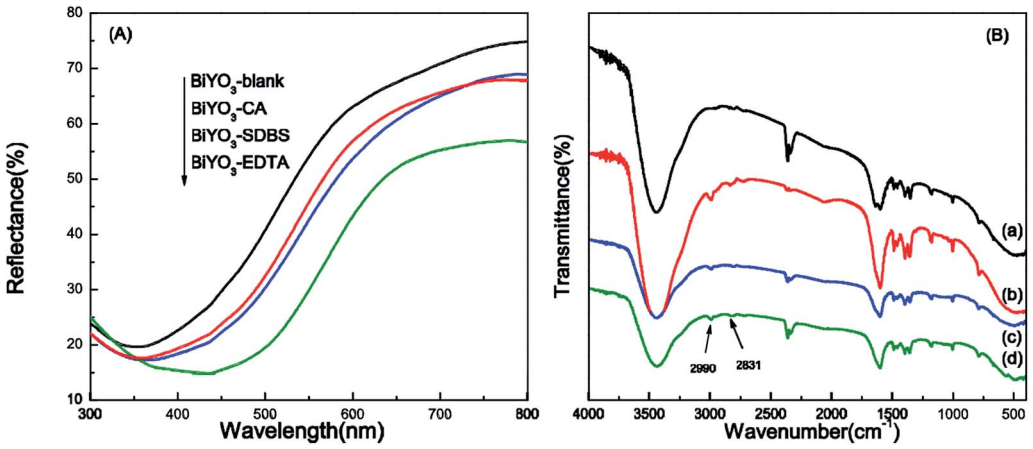

Fig. 5 UV-vis diffuse reflectance spectra (A) and FT-IR spectra (B) of the $BiYO_3$ catalysts prepared by (a) no template, and using (b) EDTA, (c) SDBS, and (d) CA as templates with a hydrothermal method.

From Fig. 6, an obvious difference in PL intensity at about 425 nm can be observed when using $BiYO_3$ prepared by different templates as photocatalysts. No PL intensity at about 425 nm was observed without a photocatalyst. The PL intensity order of the as-prepared $BiYO_3$ photocatalysts was: EDTA < SDBS < CA < no template, indicating that the addition of a template can effectively inhibit the formation of hydroxyl radicals, which were the active substances in the photocatalytic oxidation. The PL intensity of the 2-hydroxyterephthalic acid with the $BiYO_3$-EDTA photocatalyst was much lower than that of other three $BiYO_3$ photocatalysts, indicating that the $BiYO_3$ prepared by EDTA could promote the electron transfer and prevent the recombination of photogenerated electrons and holes.[49] Furthermore, the relatively lower PL intensity of $BiYO_3$-EDTA indicates that the electron–hole recombination on the surface of catalysts is largely inhibited to generate more photoelectrons and holes to trigger the photocatalytic reaction.[50]

3.7. Photocatalytic reduction of CO_2 under visible-light irradiation

Fig. 7(A) shows the HCOOH products of the $BiYO_3$ photocatalysts prepared by no template and using SDBS, EDTA, and CA as templates with a hydrothermal method. The yields of HCOOH using $BiYO_3$ prepared by no template and using SDBS, EDTA, and CA as templates were 0.90, 1.36, 1.68, and 1.06 μmol L^{-1}, respectively. For comparison, the yield of HCOOH using $BiYO_3$ prepared by a solid–state reaction was measured to be 0.64 μmol L^{-1} and there was almost no yield of HCOOH in the dark condition. Obviously, there was an enhancement of photocatalytic activity after using SDBS, EDTA, and CA as template, the yield of HCOOH by photocatalytic reduction of CO_2 by $BiYO_3$ prepared by using EDTA as template was 1.9 times higher than $BiYO_3$ prepared without template, and 2.6 times higher than that of $BiYO_3$ prepared by a solid-state reaction, or other photocatalysts, such as RuReCl,[51] and GN–TiO_2,[52] for the photocatalytic reduction of CO_2. Combined with the results of characterization, when SDBS was used as the template, the surface of the photocatalyst was covered by the adsorbed negative charges to inhibit the crystal growth, while EDTA and CA mainly formed Bi–EDTA chelation and –COOBi complexing agent with Bi^{3+} in the reaction solution to inhibit the crystal growth, then slice-like $BiYO_3$, rectangular lath-like $BiYO_3$, and scale-like $BiYO_3$ were obtained. At the same time, the addition of SDBS, EDTA, and CA also increased the specific surface area of $BiYO_3$ from 6.75 m^2 g^{-1} to 15.62, 20.87, and 12.20 m^2 g^{-1}, respectively, and decreased the band gap of the $BiYO_3$ photocatalysts from 2.39 eV to 2.32, 2.18, and 2.30 eV. Among all the $BiYO_3$ photocatalysts, the $BiYO_3$ prepared using EDTA as a template had a higher specific surface area (20.79 m^2 g^{-1}) and a larger visible light absorbed edge (569 nm) or lower band gap (2.18 eV), which greatly increased the adsorption capacity of CO_2, and provided more active sites on the catalyst surface, and accelerated the mass transfer rate of the photogenerated electron and the hole, and enhanced the separation efficiency of the photogenerated electron–hole pairs, which led to a higher photocatalytic reduction activity.[7]

The photocatalytic reduction of CO_2 can be described by eqn (2).

$$CO_2 + H_2O \leftrightarrow 1/2O_2 + HCOOH \quad (2)$$

For most of the photocatalytic processes, the kinetics can be described by a pseudo first-order reaction.[53] Therefore, using the pseudo first-order relationship between the reaction time, rate constant, and the concentration of HCOOH, the linear relationship was described by eqn (3), and Fig. 7(B) shows the plot of reaction time t and ln c.

$$\ln(c/c_0) = -kt \quad (3)$$

where c_0 is the initial concentration and c is the concentration of the HCOOH, t is the reaction time, and k is the first order rate constant. The logarithmic plot of the concentration data gives a straight line. From the data in Fig. 7(B), the reaction rate

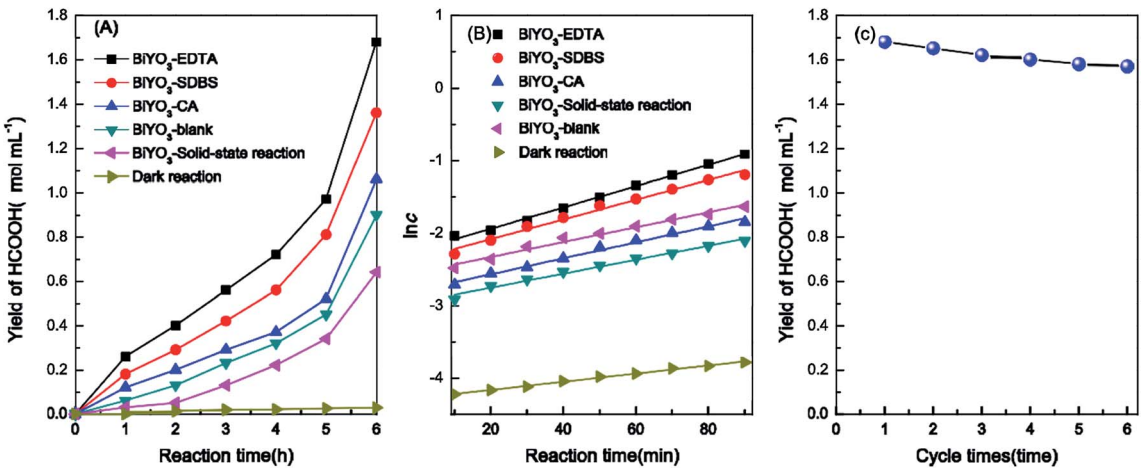

Fig. 7 (A) Yield of HCOOH, and (B) the kinetics (ln(HCOOH concentration) *vs.* reaction time) of the photocatalytic reduction of CO_2, and (C) the cycle time effect on HCOOH yield with the $BiYO_3$ catalysts prepared using EDTA as template.

constants of the photocatalytic reduction of CO_2 on $BiYO_3$ prepared using EDTA, SDBS, CA as templates and with no template, and prepared by a solid state reaction, and the reduction of CO_2 in a dark reaction were calculated to be 0.0147, 0.0136, 0.0110, 0.0102, 0.0096, and 0.0056 min^{-1}, indicating that the $BiYO_3$ prepared using EDTA exhibited the fastest reaction rate among the studied samples.

Fig. 7(C) shows the reproducibility of the $BiYO_3$ catalyst on the photocatalytic reduction of CO_2. In the same conditions, the HCOOH yield was 1.68 μmol mL^{-1} after the 1st round of reaction. When the photocatalysts were used for their sixth round, the HCOOH yield was reduced by 6.5% to 1.57 μmol mL^{-1}. This shows that the catalyst maintains a good stability after a six-time reaction. The photo-generated electrons, exhibiting strong reducing capability in the presence of H_2O, and with their reducing ability dependent on the reduction potential and the number of the transferred electrons, caused the reduction of CO_2 to HCOOH. Based on our obtained experimental results and reports in the literature,[54–55] the possible reaction mechanism for the photocatalytic reduction of CO_2 in aqueous solution is suggested in Fig. 8. The CO_2 is first absorbed on the $BiYO_3$ surface and becomes a distorted molecule. The C=O bond of absorbed CO_2 becomes long and its π bond is activated, thus, the activated C=O bond is attacked by an electron from the conduction band of $BiYO_3$ to form $\cdot CO_2^-$. The reaction of H^+ with an electron generates ·H, and the $\cdot CO_2^-$ by reaction with ·H is subsequently transformed to HCOOH.

4. Conclusions

Three templates, including SDBS, EDTA, and CA, were added to prepare $BiYO_3$ using a hydrothermal method. The effects of templates on the structure and the photocatalytic reduction properties of $BiYO_3$ were studied. The results show that, the surface area and band gap of $BiYO_3$ prepared with no template and using SDBS, EDTA, and CA as templates were 6.75, 15.62, 20.87, 12.20 $m^2\ g^{-1}$ and 2.99, 2.84, 2.64, and 2.86 eV, respectively. The addition of templates affected the production of ·OH, and the ·OH concentration was the lowest when using the $BiYO_3$ catalysts prepared by EDTA. When using $BiYO_3$ prepared by EDTA as a photocatalyst for the photocatalytic reduction of CO_2, the HCOOH yield was 1.68 μmol L^{-1}, 1.9 times higher than that produced using the $BiYO_3$ prepared with no template, and 2.6 times higher than that of $BiYO_3$ catalysts prepared by a solid-state reaction, due to the higher surface area and lower band gap, and the accelerated mass transfer rate of the photo-generated electrons and the holes.

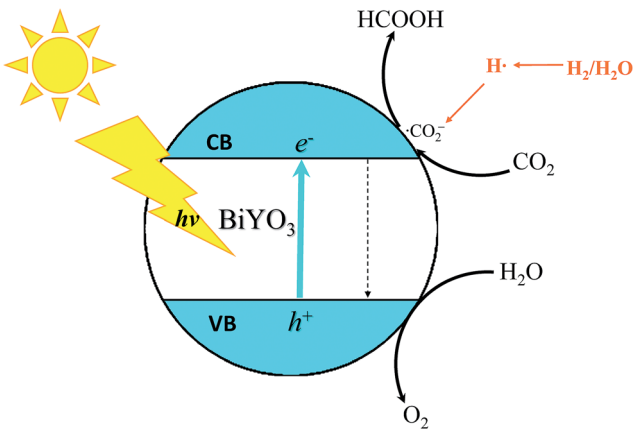

Fig. 8 Possible mechanism for the reduction of CO_2 to formic acid.

Acknowledgements

This work was supported by the National Natural Science Foundation of China (21366004, 21425627), Guangxi Zhuang Autonomous Region special funding of distinguished experts and the Open Project of Guangxi Key Laboratory of Petrochemical Resource Processing and Process Intensification Technology (2015K004).

References

1 B. K. Sovacool and P. L. Blyth, *Environ. Sci. Policy*, 2015, **54**, 304–315.
2 S. Zheng, H. Yi and H. Li, *Renewable Sustainable Energy Rev.*, 2015, **49**, 386–394.
3 D. Suryaman and K. Hasegawa, *J. Hazard. Mater.*, 2010, **183**, 490–496.
4 M. Murugananthan, M. Kumaravel, H. Katsumata, T. Suzuki and S. Kaneco, *Int. J. Hydrogen Energy*, 2015, **40**, 6740–6744.
5 Y. Zhang, C. Xu, J. Chen, X. Zhang, Z. Wang, J. Zhou and K. Cen, *Appl. Energy*, 2015, **156**, 223–229.
6 J. Mao, T. Peng, X. Zhang, K. Li and L. Zan, *Catal. Commun.*, 2012, **28**, 38–41.
7 J.-H. Kim, F. Nishimura, S. Yonezawa and M. Takashima, *J. Fluorine Chem.*, 2012, **144**, 165–170.
8 T.-m. Su, Z.-z. Qin, H.-b. Ji, Y.-x. Jiang and G. Huang, *Environ. Chem. Lett.*, 2016, **14**, 99–112.
9 M. Halmann, *Nature*, 1978, **275**, 115–116.
10 T. Inoue, A. Fujishima, S. Konishi and K. Honda, *Nature*, 1979, **277**, 637–638.
11 K. KoČÍ, K. ZatloukalovÁ, L. ObalovÁ, S. KrejČÍKovÁ, Z. LacnÝ, L. ČApek, A. HospodkovÁ and O. ŠOlcovÁ, *Chin. J. Catal.*, 2011, **32**, 812–815.
12 J. Wang, G. Ji, Y. Liu, M. A. Gondal and X. Chang, *Catal. Commun.*, 2014, **46**, 17–21.
13 H. Abdullah, M. R. Khan, M. Pudukudy, Z. Yaakob and N. A. Ismail, *J. Rare Earths*, 2015, **33**, 1155–1161.
14 P.-W. Pan and Y.-W. Chen, *Catal. Commun.*, 2007, **8**, 1546–1549.
15 X. Li, H. Pan, W. Li and Z. Zhuang, *Appl. Catal., A*, 2012, **413–414**, 103–108.
16 S. C. Yan, S. X. Ouyang, J. Gao, M. Yang, J. Y. Feng, X. X. Fan, L. J. Wan, Z. S. Li, J. H. Ye, Y. Zhou and Z. G. Zou, *Angew. Chem., Int. Ed.*, 2010, **49**, 6400–6404.
17 J. Mao, T. Peng, X. Zhang, K. Li and L. Zan, *Catal. Commun.*, 2012, **28**, 38–41.
18 R. a. He, S. Cao, P. Zhou and J. Yu, *Chin. J. Catal.*, 2014, **35**, 989–1007.
19 J. H. Sun and H. Yang, *Ceram. Int.*, 2014, **40**, 6399–6404.

20 M. Zhang, C. Shao, P. Zhang, C. Su, X. Zhang, P. Liang, Y. Sun and Y. Liu, *J. Hazard. Mater.*, 2012, **225–226**, 155–163.
21 W. Dai, H. Xu, J. Yu, X. Hu, X. Luo, X. Tu and L. Yang, *Appl. Surf. Sci.*, 2015, **356**, 173–180.
22 Z.-z. Qin, Z.-l. Liu, Y.-b. Liu and K.-d. Yang, *Catal. Commun.*, 2009, **10**, 1604–1608.
23 M.-g. Fan, Z.-z. Qin, Z.-l. Liu and T.-m. Su, *Adv. Mater. Res.*, 2011, **287–290**, 1640–1645.
24 L.-m. Xue, F.-h. Zhang, H.-j. Fan, B. Chen and X.-f. Bai, *Min. Metall. Eng.*, 2011, **31**, 84–87.
25 T.-m. Su, Z.-l. Liu, Y. Liang, Z.-z. Qin, J. Liu and Y.-q. Huang, *Catal. Commun.*, 2012, **18**, 93–97.
26 W.-t. Cheng, Z.-b. Li and J.-j. Ke, *Chin. J. of Nonferrous Met.*, 2008, **18**, 230–235.
27 S. W. Jiang, L. Yang, J. N. Pang, H. Lin and Z. Q. Wang, *Surf. Coat. Technol.*, 2016, **286**, 197–205.
28 R. Marsalek, *APCBEE Proc.*, 2014, **9**, 13–17.
29 Y. Chen, K.-c. Zhou, S.-p. Huang, Z.-y. Li and G.-c. Liu, *Chin. J. of Nonferrous Met.*, 2011, **21**, 1570–1579.
30 A. M. Dumitrescu, A. I. Borhan, A. R. Iordan, I. Dumitru and M. N. Palamaru, *Powder Technol.*, 2014, **268**, 95–101.
31 A. T. Kozakov, A. G. Kochur, A. V. Nikolsky, K. A. Googlev, V. G. Smotrakov and V. V. Eremkin, *J. Electron Spectrosc. Relat. Phenom.*, 2011, **184**, 508–516.
32 S. Poulston, N. J. Price, C. Weeks, M. D. Allen, P. Parlett, M. Steinberg and M. Bowker, *J. Catal.*, 1998, **178**, 658–667.
33 P. S. Bagus, E. S. Ilton and C. J. Nelin, *Surf. Sci. Rep.*, 2013, **68**, 273–304.
34 A. Fujimori and L. Schlapbach, *J. Phys. C: Solid State Phys.*, 1984, **17**, 341–351.
35 V. Abdelsayed, S. Moussa, H. M. Hassan, H. S. Aluri, M. M. Collinson and M. S. El-Shall, *J. Phys. Chem. Lett.*, 2010, **1**, 2804–2809.
36 L. Hu, Z. Du, X. Tai, Q. Li and Y. Zhao, *Chin. J. Catal.*, 2008, **29**, 571–576.
37 T.-m. Su, Z.-z. Qin, H.-b. Ji and Y.-x. Jiang, *Int. J. Photoenergy*, 2014, **2014**, 794057.
38 M. R. Hoffmann, S. T. Martin, W. Choi and D. W. Bahnemann, *Chem. Rev.*, 1995, **95**, 69–96.
39 K. Sutthiumporn and S. Kawi, *Int. J. Hydrogen Energy*, 2011, **36**, 14435–14446.
40 J. L. Mendoza de la Cruz, I. V. Castellanos-Ramírez, A. Ortiz-Tapia, E. Buenrostro-González, C. d. l. A. Durán-Valencia and S. López-Ramírez, *Colloids Surf., A*, 2009, **340**, 149–154.
41 H. Qi, J. Ma and P. Z. Wong, *Colloids Surf., A*, 2002, **206**, 401–407.
42 M. R. Housaindokht and A. Nakhaei Pour, *Solid State Sci.*, 2012, **14**, 622–625.
43 Z. C. Orel, M. K. Gunde and B. Orel, *Prog. Org. Coat.*, 1997, **30**, 59–66.
44 N. Guangdi, Z. Liang, L. Xiaofeng, B. Xiujie, S. Weining and W. Ce, *Dalton Trans.*, 2013, **42**, 14006–14013.
45 N. Tian, Y. Zhang, H. Huang, Y. Guo and Y. He, *Appl. Surf. Sci.*, 2014, **322**, 249–254.
46 W. Li, D. Du, T. Yan, D. Kong, J. You and D. Li, *J. Colloid Interface Sci.*, 2015, **444**, 42–48.
47 C.-Y. Chang, Y.-H. Hsieh, L.-L. Hsieh, K.-S. Yao and T.-C. Cheng, *J. Hazard. Mater.*, 2009, **166**, 897–903.
48 R. Lamba, A. Umar, S. K. Mehta, W. A. Anderson and S. K. Kansal, *J. Mol. Catal. A: Chem.*, 2015, **408**, 189–201.
49 R. J. Isaifan, S. Ntais and E. A. Baranova, *Appl. Catal., A*, 2013, **464–465**, 87–94.
50 W. Dai, H. Xu, J. Yu, X. Hu, X. Luo, X. Tu and L. Yang, *Appl. Surf. Sci.*, 2015, **356**, 173–180.
51 A. Nakada, K. Koike, T. Nakashima, T. Morimoto and O. Ishitani, *Inorg. Chem.*, 2015, **54**, 1800–1807.
52 F. Yoshitomi, K. Sekizawa, K. Maeda and O. Ishitani, *ACS Appl. Mater. Interfaces*, 2015, **7**, 13092–13097.
53 I. U. Gaya, in *Heterogeneous Photocatalysis Using Inorganic Semiconductor Solids, Springer Netherlands*, Dordrecht, 2014, pp. 43–71, DOI: 10.1007/978-94-007-7775-0_2.
54 D. Uner and M. M. Oymak, *Catal. Today*, 2012, **181**, 82–88.
55 G. Qin, Y. Zhang, X. Ke, X. Tong, Z. Sun, M. Liang and X. Song, *Appl. Catal., B*, 2013, **129**, 599–605.